Accuracy of exchange-correlation functionals and effect of solvation on the surface energy of copper

Matthew Fishman,[1] Houlong L. Zhuang,[2] Kiran Mathew,[2] William Dirschka,[2] and Richard G. Hennig[2,*]
[1]*Department of Applied and Engineering Physics, Cornell University, Ithaca, New York 14853-1501, USA*
[2]*Department of Materials Science and Engineering, Cornell University, Ithaca, New York 14853-1501, USA*
(Received 2 January 2013; revised manuscript received 12 May 2013; published 3 June 2013)

Surface energies are important for predicting the shapes of nanocrystals and describing the faceting and roughening of surfaces. Copper surfaces are of particular interest in recent years since they are the preferred surfaces for growing graphene using chemical vapor deposition. In this study we calculate the surface energies of copper for the three low-index facets (111), (100), and (110) and one high-index facet, (210), using density-functional theory with both the local-density approximation and various parametrizations of the generalized-gradient approximation to the exchange-correlation functional. To assess the accuracy of the different functionals, we obtain the average surface energies of an isotropic crystal using a broken-bond model. We use this method, which can be generalized to other crystal structures, to compare calculated surface energies to experimental surface energies for fcc crystals. We find that the recent exchange-correlation functionals AM05 and PBEsol are the most accurate functionals for calculating the surface energies of copper. To determine how solvents affect the surface energies of copper, we perform calculations using a continuum solvation model. We find that aqueous solvation changes the overall magnitude of the surface energies only slightly but leads to more isotropic surface energies.

DOI: 10.1103/PhysRevB.87.245402 PACS number(s): 68.47.De, 71.15.Mb

I. INTRODUCTION

The surface energy of solids is of fundamental importance for describing a range of phenomena involving the shape of solids and their interaction with their surroundings. For example, it is possible to model crystal growth and predict resulting shapes with available data on surface energies.[1]

Copper surfaces are of great importance because of their role as the preferred surface for chemical-vapor deposition (CVD) growth of graphene,[2] resulting in high-quality single-layer graphene with large grain sizes.[3] The main limiting factors for CVD graphene growth on copper surfaces are the facets on which graphene is grown and the roughness of the surface.[4,5] To optimize and control the growth of graphene for increased grain sizes, it is important to understand the surface faceting of the copper substrate. Copper has been shown to form steps of alternating facets,[6] which could be used to control the growth of graphene to create strips of graphene nanoribbons instead of large sheets, which presents an important step towards the creation of a variety of new graphene devices.[7]

The first step in understanding and describing the shapes and faceting of copper surfaces, and therefore allow for greater control over the growth of graphene, is to obtain accurate surface energies. The direct experimental determination of surface energies is limited because the most reliable methods do not account for the anisotropy of the energy of the facets. Additionally, the presence of solvents or surface adsorbates is difficult to control and decreases surface energies by unknown amounts.[8,9] Advancements in computational methods enable ever more accurate calculations of the energies of solids and have been used to calculate the surface energy of copper.[10] However, comparisons of the accuracy of various exchange-correlation functionals for copper surface energies, estimates of the effect of solvation, and a detailed assessment with available experimental data are still lacking.

In this work we calculate the surface energy of the three low-index (100), (110), and (111) facets and the facet with the highest energy, the high-index (210) facet of copper,[11–13] using density-functional theory (DFT) for various approximations to the exchange-correlation functional. To compare with experimental data, we use a broken-bond model to estimate the average surface energy of a spherical copper crystal, which we find to be approximately equal to the surface energy of the (110) facet for fcc crystals. This novel approach enables us to compare computed surface energies to experimental surface energies. We find that two recently developed generalized-gradient approximations (GGAs; AM05 and PBEsol) perform significantly better than the local-density approximation (LDA) and previous GGAs (PBE and PW91). To determine how solvents affect the surface energies of copper, we perform calculations using a polarizable continuum model for the solvent.[14–16] We find that solvation in water changes the overall magnitude of the surface energies only slightly but results in more isotropic surface energies.

The organization of this paper is as follows. Section II presents the details of the computational methods. Section III reports the results for the bulk and surface calculations for the different functionals under investigation. In Sec. IV, a broken-bond model is fit to the calculation. The model is used to estimate the surface energy averaged over all high-index surfaces to compare the results of various exchange-correlation functionals to available experimental measurements. Finally, Sec. V summarizes the work.

II. COMPUTATIONAL METHODS

Our calculations are performed using DFT[17] with a plane-wave basis set and the projector-augmented wave method as implemented in the Vienna *ab initio* simulation package[18,19] (VASP). A cutoff energy of 460 eV for the plane-wave basis set is used throughout all calculations. We calculate the surface energies of copper using the LDA[20] and various forms of the GGA to the exchange-correlation functional. The GGA exchange-correlation functionals we test are PW91,[21] PBE,[22]

and the more recent AM05[23] and PBEsol.[24] The AM05 and PBEsol functionals are specifically designed for surfaces of materials.

For all functionals we converge the bulk and surface energies with respect to the k-point mesh and cutoff energy to ensure the accuracy of our results. We converge the total energy to less than 1 meV/atom and the surface energy to an accuracy of about 1%.

For the calculations of the lattice parameter, the cohesive energy, the bulk modulus, and its pressure derivative we use a $16 \times 16 \times 16$ k-point mesh. The cohesive energy is obtained as the energy difference between the relaxed bulk phase and a spin-polarized atom in a cubic simulation cell with a 10-Å edge length using the Γ point. The equilibrium lattice parameter, a_0, the bulk modulus, B, and its pressure derivative, B_0', are obtained by fitting the Birch equation of state to the energy as a function of volume.[25,26]

The surface energies are calculated from two calculations using the same simulation cells, one corresponding to a slab of seven atomic layers and the second using the same simulation cell but filled with Cu atoms in the bulk fcc structure. For both cells we fix the lattice parameter to the relaxed value from the bulk calculation for the respective functional. For both cells we use the same $16 \times 16 \times 1$ k-point mesh. The AM05 functional requires the slightly smaller vacuum spacing of 7 Å to obtain self-consistency in the DFT calculations and to overcome instabilities caused by the large vacuum region required for surface energy calculations.[34] For all of the other functionals for all facets we use a vacuum spacing of at least 10 Å to minimize the interaction between the slabs. The surfaces are allowed to relax, with the middle layers held fixed and the top and bottom two layers allowed to move. Figure 1 shows the convergence of the surface energy with respect to the number of layers for the (111) facet using the PBE functional. As shown in Fig. 1, increasing the number of bulk copper layers from 7

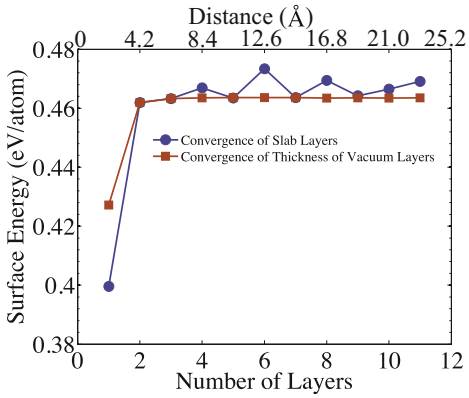

FIG. 1. (Color online) An example of the convergence of the surface energy per atom of a Cu (111) surface with respect to the number of slab layers and vacuum layers using the PBE functional. Seven layers of vacuum are used for the slab convergence test, while seven slab layers are used for the vacuum convergence test. The surface energy per atom converges very rapidly, with almost no change after two vacuum layers, indicating minimal interlayer interaction if just two or more vacuum layers are used. The surface energy converges very rapidly as well, and changes by only about 1% when the number of layers is increased from 7 to 11.

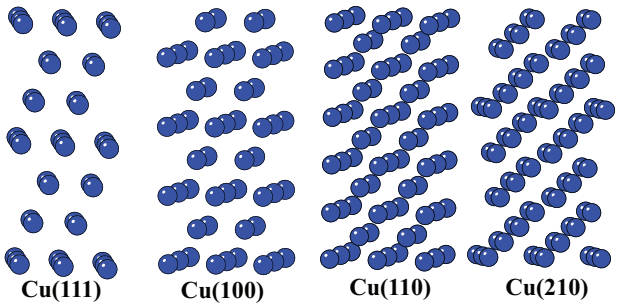

FIG. 2. (Color online) Unrelaxed (111), (100), (110), and (210) surface structures of Cu visualized using VMD.[27] Geometries are shown with 7, 8, 11, and 17 layers for the (111), (100), (110), and (210) surfaces, respectively. These are the geometries used for surface energy calculations with the PW91, PBE, PBEsol, and LDA functionals. For the AM05 functional, we used geometries with 9, 11, 13, and 21 layers but the same overall unit cell size to decrease the vacuum space in order to overcome instabilities caused by the large vacuum region. At the surface the coordination number is reduced from 12 to 9, 8, 7, and 6 nearest neighbors for the (111), (100), (110), and (210) surfaces, respectively. For the second layer of the (110) surface, the coordination number is reduced to 11 nearest neighbors. The coordination numbers of the second and third layers of the (210) surface are 9 and 11. The layer spacing for the (111), (100), (110), and (210) surfaces is $a_0/\sqrt{3}$, $a_0/2$, $a_0/(2\sqrt{2})$, and $a_0/(2\sqrt{5})$. In general for a surface (hkl) the spacing is $a_0/\sqrt{h^2+k^2+l^2}$ if h, k, and l are all odd and $a_0/(2\sqrt{h^2+k^2+l^2})$ otherwise.

to 11 changes the surface energy by about 1%. Our results are similar to previous work by Da Silva *et al.*[10] Figure 2 shows the unrelaxed surface geometries for all four facets being studied.

To estimate the effect of solvation we implemented a continuum solvation model[14,15] into the VASP code.[16] This model modifies the electrostatic potential of the electrons and nuclei to account for the polarization of the solvent molecules due to the electric field from the solute. We employ a linear polarization model with a permittivity that increases smoothly from a value of 1 inside the volume of the solute to the permittivity of the solvent ϵ_{solv} away from the solute.[14] The modified Hartree potential is obtained from the modified Poisson equation

$$\nabla \cdot (\epsilon(\mathbf{r})\nabla\phi(\mathbf{r})) = -4\pi n(\mathbf{r}), \tag{1}$$

where $n(\mathbf{r})$ is the charge density and the permittivity $\epsilon(\mathbf{r})$ is assumed to be a continuous function of the valence charge density of the solid. The mean-field solvent potential through the density dependence becomes itself a functional of the electron density and is calculated self-consistently. Using this approach we calculate how the presence of water with a relative permittivity of $\epsilon_{\text{solv}} = 80$ at 20 °C affects the surface energies of the Cu facets.

III. RESULTS

A. Bulk properties

Table I compares the calculated bulk properties for the PW91, PBE, AM05, PBEsol, and LDA functionals with experimental data that was corrected by Csonka *et al.* for zero-point phonon effects.[28] Similar numbers have been reported by others, such as by Kambe[35] for the lattice constant (3.60 Å)

TABLE I. Comparison of our calculated bulk properties of copper with experiments. The table includes the equilibrium lattice parameter a_0, the bulk modulus B_0, the pressure derivative of the bulk modulus B_0', and the cohesive energy E_{coh} for the functionals PW91, PBE, AM05, PBEsol, and LDA (listed in the same order as in Table II, the order of increasing surface energy). The numbers in boldface are those which are closest to the shown experimental values. Our calculations of B_0' are within the range of those measured experimentally.

	PW91	PBE	AM05	PBEsol	LDA	Expt.
a_0 (Å)	3.646	3.649	**3.577**	**3.579**	3.532	3.595[a]
B_0 (GPa)	**134.6**	**133.2**	156.2	160.4	177.7	142[a]
B_0'	4.678	4.500	4.954	5.010	5.254	3.91–5.8[b]
E_{coh} (eV/atom)	**3.517**	**3.503**	3.783	4.046	4.548	3.524[a]

[a]From Ref. 28.
[b]Range of experimental values from Refs. 29–33.

and cohesive energy (3.52 eV/atom) and by Chelikowsky and Chou[36] for the lattice constant (3.50 Å), bulk modulus (142 GPa), and cohesive energy (3.50 eV/atom). We find, as is often observed, that the GGA functionals PW91 and PBE slightly overestimate the equilibrium lattice constant, while AM05 and PBEsol slightly underestimate it. We find that the calculated equilibrium lattice constants from the AM05 and the PBEsol functional agree slightly better with experimental data than those from the PW91 or the PBE functional. The LDA functional underestimates the equilibrium lattice constant and appears to be the least accurate functional of the ones studied. For the bulk modulus, the GGA functionals PW91 and PBE are the most accurate. The calculated pressure derivatives of the bulk modulus of copper, B_0', for all functionals are well within the wide range of experimental values of 3.91–5.8 reported in the literature.[30–33]

B. Surface properties

Table II reports the calculated surface energies for the three low-index facets (111), (100), and (110) and the high-index facet (210). For all of the functionals, $\gamma_{111} < \gamma_{100} < \gamma_{110} < \gamma_{210}$, which is consistent with the predictions of the broken-bond model described in Sec. IV. The GGA functionals, PW91 and PBE, provide the lowest surface energies, while the new GGA functionals, AM05 and PBEsol, result in higher surface energies. The LDA functional predicts the highest surface energies for all four facets. Table II also shows the ratio of the surface energies of the (hkl) facet relative to the lowest energy (111) facet. These ratios are a measure of the anisotropy of the surface energy and are almost the same for all of the tested functionals. Also shown are the percentage relaxations Δ_{ij}, defined as the percentage change in the distance between layer i and layer j (where 1 is the top layer) in the relaxed and unrelaxed configuration. The percentage relaxations Δ_{12} and Δ_{23} are similar for all of the functionals we tested. For all functionals, the relaxations occur in the same direction as is experimentally observed, with the exception that AM05 predicts a contraction for Δ_{23} for all of the facets, while expansions are observed experimentally. The calculated relaxations are in general somewhat larger than measured, particularly for the top layer relaxation Δ_{12}.

Figure 3 and Table II compare the calculated surface energies to the average surface energies extrapolated from high-temperature measurements. Tyson and Miller estimate a value of 1.790 J/m^2 for the surface energy of copper.[9]

TABLE II. Comparison of the calculated surface energies and relaxations of copper to experimental values. Listed are the surface energies γ_{hkl} in units of both J/m^2 and eV/atom for the three low-index (111), (100), and (110) facets and the high-index (210) facet for the functionals PW91, PBE, AM05, PBEsol, and LDA. Functionals are listed in order of increasing surface energy. Surface energy anisotropy ratios relative to the lowest energy (111) surface, $\gamma_{hkl}/\gamma_{111}$, are also listed. The ratios are taken using the surface energy per area. These ratios are very similar for the different functionals. Also listed are the percentage relaxation values of the first and second layers (Δ_{12}) and of the second and third layers (Δ_{23}) for each facet and functional. A negative value indicates that the space between the layers contracted, while a positive number indicates that the space between the layers expanded.

Surface		PW91	PBE	AM05	PBEsol	LDA	Expt.
γ_{111}	J/m^2 (eV/atom)	1.273 (0.455)	1.289 (0.461)	1.506 (0.518)	1.609 (0.554)	1.760 (0.591)	
γ_{100}	J/m^2 (eV/atom)	1.442 (0.595)	1.458 (0.602)	1.672 (0.664)	1.806 (0.718)	1.981 (0.768)	
γ_{110}	J/m^2 (eV/atom)	1.532 (0.894)	1.551 (0.905)	1.798 (1.010)	1.913 (1.076)	2.096 (1.149)	1.790,[a] 1.825[b]
γ_{210}	J/m^2 (eV/atom)	1.557 (1.438)	1.578 (1.456)	1.854 (1.647)	1.954 (1.738)	2.141 (1.855)	
	$\gamma_{100}/\gamma_{111}$	1.132	1.131	1.110	1.123	1.126	
	$\gamma_{110}/\gamma_{111}$	1.203	1.204	1.194	1.189	1.191	
	$\gamma_{210}/\gamma_{111}$	1.223	1.224	1.231	1.214	1.216	
(111)	Δ_{12} (%)	−1.00	−0.78	−1.37	−0.89	−1.16	−0.3 to −0.7[c]
	Δ_{23} (%)	+0.01	+0.33	−0.15	+0.29	+0.00	
(100)	Δ_{12} (%)	−3.05	−2.77	−3.76	−2.73	−2.91	−1.0 to −2.1[c]
	Δ_{23} (%)	+0.96	+0.95	−0.20	+0.86	+0.85	+0.45 to +2.0[c]
(110)	Δ_{12} (%)	−10.26	−9.73	−10.21	−9.70	−10.15	−5.3 to −10.0[c]
	Δ_{23} (%)	+3.57	+3.38	+2.49	+3.24	+3.37	+0.0 to +3.3[c]
(210)	Δ_{12} (%)	−17.33	−16.58	−16.01	−15.85	−16.91	
	Δ_{23} (%)	+0.04	+0.07	−2.19	−0.60	−0.29	

[a]Average surface energy extrapolated to $T = 0$ from liquid surface tension data of Tyson and Miller[9] (in J/m^2).
[b]Average surface energy extrapolated to $T = 0$ from liquid surface tension data of Boer[37] (in J/m^2).
[c]Experimental numbers compiled by Wan *et al.*[38] from various sources.

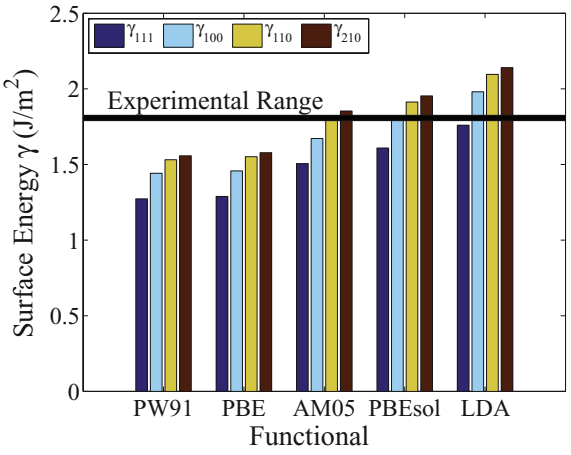

FIG. 3. (Color online) Comparison of the surface energies for various functionals with the range of experimental values of 1.790–1.825 J/m^2.[9,37] The measured values correspond to an average surface energy of copper, which is expected to be bound between the lowest and the highest surface energies, γ_{111} and γ_{210}. Our analysis using the broken-bond model in Sec. IV shows that the average surface energy should be close to γ_{110}, indicating that the AM05 and PBEsol functionals are the most accurate methods studied here.

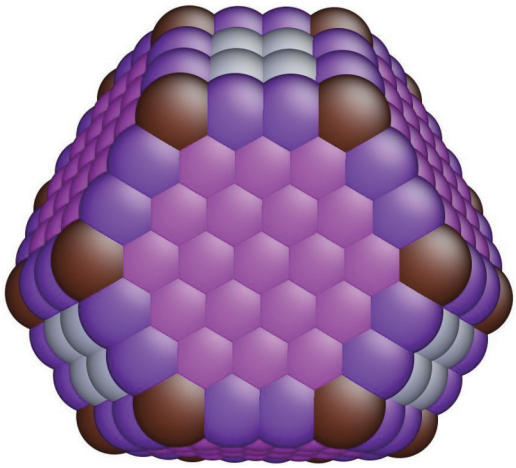

FIG. 4. (Color online) Shape of copper nanocrystal predicted by the Wulff construction using the surface energies calculated by PBEsol (from Table II). The Wulff construction predicts very similar nanoparticles for the other functionals under investigation. Only the two lowest energy facets, (111) and (100), are predicted to occur. Atoms are colored by the number of nearest neighbors [nine for atoms on the (111) surface and eight for atoms on the (100) surface]. The nanocrystal is visualized using the AtomEye package.[39]

Their approach is based on available experimental data for the liquid surface tension, γ_{LV}, which is considered more reliable than direct experimental measurements of the surface energy because it is difficult to control for surface contaminants, which decrease the surface energy by unknown amounts. Tyson and Miller derive an expression for the solid surface energy at the melting point, $\gamma(T_m)$, as a function of the liquid surface tension, γ_{LV}, and the solid-liquid interfacial energy, γ_{SL}, of the metals and determine the solid surface energy using an estimate for the ratio γ_{SL}/γ_{LV}. They estimate that $\gamma(T_m) \approx 1.18\gamma_{LV}$ for all metals and extrapolate the surface energy to low temperatures using an estimate for the surface entropy. This results in $\gamma(T) \approx \gamma(T=0) + k_B T/A$, where $A \approx 1.162 N_A^{1/3} V_m^{2/3}$ (k_B is the Boltzmann constant, N_A is Avogadro's number, and V_m is the molar volume). For copper, they calculate that $\gamma(T_m)$ is 1.566 J/m^2 and RT_m/A is 0.224 J/m^2, leading to a surface energy of copper at zero temperature of 1.1790 J/m^2. The estimate by Tyson and Miller provides an average surface energy[9] and does not provide any information about the anisotropy of the surface energies. This evidently hinders a direct comparison with our calculations.

In Fig. 3 we compare our calculated surface energies with the average surface energy obtained by Tyson and Miller[9] and a second experimental value of 1.825 J/m^2 by Boer,[37] which also approximates the surface energy using the liquid surface tension of copper. The average surface energy is expected to fall between the lowest and the highest surface energies, γ_{111} and γ_{210}. The PW91 and PBE functionals predict surface energies for all facets below the experimental values, so they evidently underestimate the surface energy of copper. For LDA, the experimental values fall near the lowest energy surface, γ_{111}. The average surface energy would be expected to be somewhat higher, within the range of surface energies between γ_{111} and γ_{210}, and indeed is expected to fall near γ_{110} as we show with the broken-bond model in Sec. IV. So LDA evidently overestimates the surface energy of copper. For AM05 and PBEsol, the experimental value is right in between the calculated γ_{111} and γ_{210}, indicating that the AM05 and PBEsol functionals are the most accurate functionals in our study. For a quantitative comparison with the experimental data, we estimate the average surface energy using the calculated surface energies of the four facets by a broken-bond model in Sec. IV.

Figure 4 shows the predicted shape of a copper nanocrystal from the Wulff construction using the surface energies from the PBEsol functional. The predicted shapes for the other functionals are very similar, as expected from the nearly identical anisotropy ratios calculated with the different functionals as reported in Table II. Only the (111) and (100) facets, the lowest energy facets, are predicted to show on the nanocrystal. The shape is consistent with that predicted by Duan *et al.* for clean surfaces.[40] In their paper they predict that the shape changes significantly for different levels of oxygen adsorption on the surface.

To study how the environment affects the surface energies and shape of nanocrystals, we determine the change in energy of the copper surfaces when the material is solvated in water. Table III lists the resulting solvation energies. The presence of water reduces the surface energies by small amounts, ranging from 15 to 85 meV/atom. Interestingly, solvation reduces

TABLE III. Effect of aqueous solvation on the surface energy of copper facets.

	Facet			
	(111)	(100)	(110)	(210)
Solvation energy				
J/m^2	−0.045	−0.053	−0.083	−0.095
eV/atom	−0.015	−0.021	−0.047	−0.085

the energy of the higher energy facets by a larger amount, effectively reducing the anisotropy of the surface energies. This can be understood since the electrostatic screening is more effective for Cu atoms with lower coordination numbers.

IV. AVERAGE SURFACE ENERGY AND THE BROKEN-BOND MODEL

To compare our calculated surface energies with estimates based on high-temperature measurements of the average surface energy, we calculate the average surface energy of a spherical copper crystal using a broken-bond model. The broken-bond models estimate the surface energy of a crystal based on the number of broken bonds. In this section we start with a surface energy expression from Mackenzie *et al.*[41] to derive an expression for the average surface energy. We start by using their approximation that the surface energy per area is given by the number of broken bonds per surface area multiplied by the energy associated with each bond, and average the expression over a unit sphere.

A. First-nearest-neighbor approximation

The surface energy as a function of the Miller indices for an fcc crystal according to the broken-bond model counting only nearest neighbors is

$$\gamma_{\mathbf{h}} = \gamma_{hkl} = \frac{E_{\mathrm{b}}}{2\Omega|\mathbf{h}|}\,\mathbf{h}\cdot(2,1,0), \tag{2}$$

where $E_b = E_{\mathrm{coh}}/12$ is the energy per bond (using the coordination number of 12 for fcc), $\Omega = a_0^2/4$ is the volume per atom in the primitive unit cell for an fcc crystal divided by the lattice constant a_0, and $\mathbf{h}/|\mathbf{h}|$ is the surface normal vector for the facet (hkl),

$$\frac{\mathbf{h}}{|\mathbf{h}|} = \frac{(h,k,l)}{\sqrt{h^2+k^2+l^2}}. \tag{3}$$

It is important to note that Eq. (2) only holds assuming the following relationship between the Miller indices:

$$h \geqslant k \geqslant l \geqslant 0. \tag{4}$$

The motivation for these equations and relations can be found in Mackenzie's original paper.[42]

Some important trends of the surface energy can immediately be gleamed from Eq. (2). First, by taking the gradient of this equation with respect to (h,k,l) and setting it equal to 0, it can be shown that $\mathbf{h} = (2,1,0)$ gives the maximum surface energy and therefore γ_{210} provides an upper bound on the average surface energy. Various theoretical studies corroborate that the (210) facet exhibits the highest surface energy of any facet for fcc copper.[11–13] Hence as mentioned earlier, the experimental estimate of the surface energy must fall within the range of calculated surface energies between γ_{111} and γ_{210}.

Next, we examine the predicted anisotropy of the surface energies relative to the lowest energy (111) surface,

$$\frac{\gamma_{\mathbf{h}}}{\gamma_{111}} = \frac{\sqrt{3}}{3}\frac{(2h+k)}{\sqrt{h^2+k^2+l^2}}. \tag{5}$$

These ratios determine the shape of the copper nanocrystals and are independent of the cohesive energy. Figure 5 and

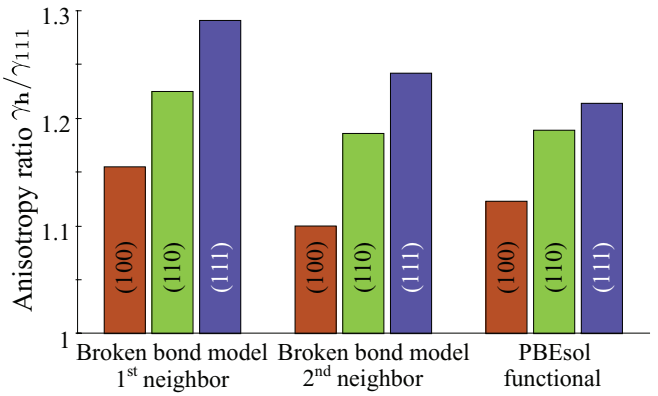

FIG. 5. (Color online) Comparison of the prediction of the broken-bond models for the anisotropy ratios relative to the (111) surface energy $\gamma_{\mathbf{h}}/\gamma_{111}$ with the calculation using the PBEsol functional. Both models describe the trend of the surface energies well, with the second-nearest-neighbor broken-bond model being most accurate.

Table IV show that the parameter-free prediction of the first-nearest-neighbor broken-bond model correctly predicts the trend of the surface energies $\gamma_{210} > \gamma_{110} > \gamma_{100} > \gamma_{111}$ and quantitatively agrees within about 4% with the calculated values for the PBEsol functional.

To compare with the experimentally estimated average surface energy, we calculate the average surface energy of a spherical copper crystal, γ_{ave}, using the first-nearest-neighbor broken-bond model. For brevity we define a constant,

$$\gamma_0 \equiv \frac{E_{\mathrm{b}}}{2\Omega} = \frac{E_{\mathrm{coh}}/12}{2a_0^2/4}, \tag{6}$$

so that Eq. (2) becomes

$$\gamma_{hkl} = \frac{2h+k}{\sqrt{h^2+k^2+l^2}}\gamma_0. \tag{7}$$

For convenience we use spherical polar coordinates,

$$h = |\mathbf{h}|\cos\theta\cos\phi, \tag{8}$$

$$k = |\mathbf{h}|\sin\theta\cos\phi, \tag{9}$$

$$l = |\mathbf{h}|\sin\phi, \tag{10}$$

TABLE IV. Anisotropy ratios relative to the (111) surface energy, $\gamma_{\mathbf{h}}/\gamma_{111}$, for the nearest-neighbor and second-nearest-neighbor broken-bond model compared to the calculated values for the PBEsol functional. Both models describe the trend of the surface energies well, with the second-nearest-neighbor broken-bond model being the more accurate.

Facet	1st-nearest-neighbor broken-bond model	2nd-nearest-neighbor broken-bond model	PBEsol
(100)	$\frac{2}{\sqrt{3}} \approx 1.155$	1.102	1.123
(110)	$\sqrt{\frac{3}{2}} \approx 1.225$	1.188	1.189
(210)	$\sqrt{\frac{5}{3}} \approx 1.291$	1.244	1.214

where ϕ is the angle off of the $\hat{l}$ axis and θ is the angle in the $\hat{h}$-$\hat{k}$ plane off of the $\hat{h}$ axis. Equation (7) in polar coordinates becomes

$$\gamma(\theta,\phi) = [(2\cos\theta + \sin\theta)\sin\phi]\gamma_0. \tag{11}$$

The change to polar coordinates modifies the inequality given by Eq. (4) to

$$\cos\theta\sin\phi \geqslant \sin\theta\sin\phi \geqslant \cos\phi \geqslant 0, \tag{12}$$

which leads to the following constraints on θ and $\cos\phi$:

$$0 \leqslant \theta \leqslant \frac{\pi}{4}, \tag{13}$$

$$0 \leqslant \cos\phi \leqslant \frac{1}{\sqrt{\csc^2\theta + 1}}. \tag{14}$$

The first inequality constraining θ results from $\cos\theta \geqslant \sin\theta \geqslant 0$ and the second inequality constraining ϕ results from $\sin\theta\sin\phi \geqslant \cos\phi \geqslant 0$.

To obtain the average surface energy we integrate the expression for the surface energy given by Eq. (11) over the section of the sphere given by the above constraints and divide that by the corresponding surface area of that same section of the sphere:

$$\gamma_{\text{ave}} = \frac{\int_0^{\frac{\pi}{4}} d\theta \int_0^{\frac{1}{\sqrt{\csc^2\theta+1}}} d(\cos\phi)\gamma(\theta,\cos\phi)}{\int_0^{\frac{\pi}{4}} d\theta \int_0^{\frac{1}{\sqrt{\csc^2\theta+1}}} d(\cos\phi)}. \tag{15}$$

Evaluating these integrals gives a surprisingly simple result:

$$\gamma_{\text{ave}} = \frac{\pi/4\sqrt{2}}{\pi/12}\gamma_0 = \frac{3}{\sqrt{2}}\gamma_0. \tag{16}$$

This is a remarkable result because the predicted average surface energy of a spherical copper crystal is exactly the same as that predicted by the broken-bond model for the (110) facet! In short, the broken-bond model accounting only for nearest-neighbor interactions predicts that $\gamma_{\text{ave}} = \gamma_{110}$ for *any* fcc crystal.

The broken-bond model provides a simple way to evaluate the accuracy of different functionals for the surface energy, which is to merely compare the experimental surface energy data to the calculated surface energy of the (110) facet. Table II and Fig. 3 show that γ_{110} is closest to the experimental values for the AM05 and PBEsol functionals, which are the most accurate methods for calculating the surface energy of copper, while the PW91 and PBE functionals both underestimate the surface energies and the LDA functional overestimates them.

B. Second-nearest-neighbor approximation

The broken-bond model can be improved by including second nearest neighbors, resulting in the surface energies

$$\gamma_{hkl} = \frac{E_{\text{b}}}{2\Omega|\mathbf{h}|}\mathbf{h}\cdot[(2,1,0) + (2,2,2)\,\rho], \tag{17}$$

where the parameter ρ represents the ratio of the second-nearest-neighbor bond energy to the first-nearest-neighbor bond energy, E_{b}. The value of ρ can be estimated using calculations for the cohesive energy and one surface energy. Using the lowest surface energy, γ_{111}, we get

$$\gamma_{111} = \frac{(E_{\text{coh}}/12)}{2(a_0^2/4)\sqrt{3}}[3 + 6\rho]. \tag{18}$$

With the values of the PBEsol functional ($\gamma_{111} = 1.609$ J/m^2, $E_{\text{coh}} = 4.046$ eV, and $a_0 = 3.577$ Å), we obtain $\rho \approx 0.050$. Figure 5 and Table IV show that including the second nearest neighbors in the broken-bond model further improves the agreement of the anisotropy ratios with the calculations.

Following the same steps as in Sec. IV A we obtain the average surface energy of a spherical copper crystal for the broken-bond model including second nearest neighbors:

$$\gamma_{\text{ave}} = \left(\frac{3}{\sqrt{2}} + 3\rho\right)\gamma_0. \tag{19}$$

The anisotropy ratio for the average surface energy taking into account second-nearest-neighbor interactions becomes $\gamma_{\text{ave}}/\gamma_{111} \approx 1.192$, which is very close to the anisotropy ratio for the (110) facet of $\gamma_{110}/\gamma_{111} \approx 1.188$. Again, comparing the surface energy γ_{110} to the experimental estimate provides a good measure of the accuracy of different functionals for the surface energy. Hence, our earlier conclusions for the accuracy of the different functionals for the surface energies are unchanged when including second-nearest-neighbor interactions in the broken-bond model, i.e., the PBEsol and AM05 functionals are the most accurate of those studied.

This broken-bond method can easily be generalized. It can be applied to any fcc material and extended to bcc and other crystal structures as well by using modified expressions for the first- and second-nearest-neighbor broken-bond model surface energies. A comparison with experimental estimates requires only the calculation of either the cohesive energy or a single surface energy when using the first-nearest-neighbor approximation of the broken-bond model. Using the significantly more accurate second-nearest-neighbor approximation requires as input two pieces of data, either the cohesive energy and one surface energy or two surface energies.

V. CONCLUSION

In this study we have calculated the surface energy of the three low-index facets (111), (100), and (110) and one high-index facet, (210), of copper for various approximations of the exchange-correlation functional and compared our results to reliable experimental estimates. To compare with experimental data, we have used a broken-bond model to derive an estimate for the average surface energy of a spherical copper crystal, which we found to be approximately equal to the surface energy of the (110) facet for fcc crystals. Using this approach we compare the computed surface energies to the experimental average surface energies. We find that the more recent GGA functionals, AM05 and PBEsol, designed for bulk and surface calculations, are the most accurate for calculating the surface energies of copper, while the PW91 and PBE functionals perform better for the bulk modulus and cohesive energy. The PW91 and PBE functionals yield surface energies below the experimental values, while the LDA calculates surface energies that are too high.

All functionals predicted similar percentage relaxations of the top two layers, which are generally consistent, albeit

somewhat larger, than the available experimental data. The surface energy anisotropy ratios for the different functionals are all very similar and agree with the predictions of the broken-bond model including both first- and second-nearest-neighbor interactions. Hence, the shapes of copper nanocrystals predicted by the Wulff construction are essentially the same for the different functionals.

We determined the effect of solvent on the surface energies using a continuum solvation model we implemented into the VASP code. We predict that the presence of water slightly reduces the overall surface energies of all facets, with larger reductions observed for the higher energy facets. We hope that our method of using the broken-bond model to compare calculated surface energies to the available experimental data and our approach of determining the effect of solvents on surface energies using a continuum solvation model will improve the accuracy of future surface energy calculations.

ACKNOWLEDGMENTS

This work was supported by the National Science Foundation through the Cornell Center for Materials Research under Award No. DMR-1120296, CAREER Award No. DMR-1056587, and the Energy Materials Center at Cornell (EMC2) funded by the US Department of Energy, Office of Basic Energy Sciences, under Award No. DE-SC0001086. This research used computational resources of the Texas Advanced Computing Center under Contract No. TG-DMR050028N and of the Computation Center for Nanotechnology Innovation at Rensselaer Polytechnic Institute.

*rhennig@cornell.edu

[1] C. R. Bealing, W. J. Baumgardner, J. J. Choi, T. Hanrath, and R. G. Hennig, ACS Nano **6**, 2118 (2012).
[2] C. Mattevi, H. Kim, and M. Chhowalla, J. Mater. Chem. **21**, 3324 (2011).
[3] X. Li, W. Cai, J. An, S. Kim, J. Nah, D. Yang, R. Piner, A. Velamakanni, I. Jung, E. Tutuc, S. K. Banerjee, L. Colombo, and R. S. Ruoff, Science **324**, 1312 (2009).
[4] G. H. Han, F. Gnes, J. J. Bae, E. S. Kim, S. J. Chae, H.-J. Shin, J.-Y. Choi, D. Pribat, and Y. H. Lee, Nano Lett. **11**, 4144 (2011).
[5] J. D. Wood, S. W. Schmucker, A. S. Lyons, E. Pop, and J. W. Lyding, Nano Lett. **11**, 4547 (2011).
[6] S. Vollmer, A. Birkner, S. Lukas, G. Witte, and C. Woll, Appl. Phys. Lett. **76**, 2686 (2000).
[7] L. C. Campos, V. R. Manfrinato, J. D. Sanchez-Yamagishi, J. Kong, and P. Jarillo-Herrero, Nano Lett. **9**, 2600 (2009).
[8] L. Vitos, A. Ruban, H. Skriver, and J. Kollár, Surf. Sci. **411**, 186 (1998).
[9] W. Tyson and W. Miller, Surf. Sci. **62**, 267 (1977).
[10] J. L. F. Da Silva, C. Stampfl, and M. Scheffler, Surf. Sci. **600**, 703 (2006).
[11] X. Wang, Y. Jia, Q. Yao, F. Wang, J. Ma, and X. Hu, Surf. Sci. **551**, 179 (2004).
[12] Y.-N. Wen and J.-M. Zhang, Solid State Commun. **144**, 163 (2007).
[13] J. L. F. Da Silva, C. Barreteau, K. Schroeder, and S. Blügel, Phys. Rev. B **73**, 125402 (2006).
[14] S. A. Petrosyan, A. A. Rigos, and T. A. Arias, J. Phys. Chem. B **109**, 15436 (2005).
[15] S. A. Petrosyan, J.-F. Briere, D. Roundy, and T. A. Arias, Phys. Rev. B **75**, 205105 (2007).
[16] K. X. Mathew, R. Sundararaman, K. Letchworth-Weaver, T. A. Arias, and R. G. Hennig (submitted for publication, 2013).
[17] W. Kohn and L. J. Sham, Phys. Rev. **140**, A1133 (1965).
[18] G. Kresse and J. Furthmüller, Phys. Rev. B **54**, 11169 (1996).
[19] G. Kresse and D. Joubert, Phys. Rev. B **59**, 1758 (1999).
[20] J. P. Perdew and Y. Wang, Phys. Rev. B **45**, 13244 (1992).
[21] J. P. Perdew, J. A. Chevary, S. H. Vosko, K. A. Jackson, M. R. Pederson, D. J. Singh, and C. Fiolhais, Phys. Rev. B **46**, 6671 (1992).
[22] J. P. Perdew, K. Burke, and M. Ernzerhof, Phys. Rev. Lett. **77**, 3865 (1996).
[23] R. Armiento and A. E. Mattsson, Phys. Rev. B **72**, 085108 (2005).
[24] J. P. Perdew, A. Ruzsinszky, G. I. Csonka, O. A. Vydrov, G. E. Scuseria, L. A. Constantin, X. Zhou, and K. Burke, Phys. Rev. Lett. **100**, 136406 (2008).
[25] F. Birch, Phys. Rev. **71**, 809 (1947).
[26] E. Ziambaras and E. Schröder, Phys. Rev. B **68**, 064112 (2003).
[27] W. Humphrey, A. Dalke, and K. Schulten, J. Mol. Graph. **14**, 33 (1996).
[28] G. I. Csonka, J. P. Perdew, A. Ruzsinszky, P. H. T. Philipsen, S. Lebègue, J. Paier, O. A. Vydrov, and J. G. Ángyán, Phys. Rev. B **79**, 155107 (2009).
[29] D. Lazarus, Phys. Rev. **76**, 545 (1949).
[30] W. B. Daniels and C. S. Smith, Phys. Rev. **111**, 713 (1958).
[31] K. Salama and G. A. Alers, Phys. Rev. **161**, 673 (1967).
[32] R. Chiarodo, J. Green, I. Spain, and P. Bolsaitis, J. Phys. Chem. Solids **33**, 1905 (1972).
[33] S. Narasimhan and S. de Gironcoli, Phys. Rev. B **65**, 064302 (2002).
[34] M. J. Piotrowski, P. Piquini, M. M. Odashima, and J. L. F. Da Silva, J. Chem. Phys. **134**, 134105 (2011).
[35] K. Kambe, Phys. Rev. **99**, 419 (1955).
[36] J. R. Chelikowsky and M. Y. Chou, Phys. Rev. B **38**, 7966 (1988).
[37] F. Boer, *Cohesion in Metals: Transition Metal Alloys* (*Cohesion and Structure*) (North-Holland, Amsterdam, 1988).
[38] J. Wan, Y. L. Fan, D. W. Gong, S. G. Shen, and X. Q. Fan, Model. Simul. Mater. Sci. Eng. **7**, 189 (1999).
[39] J. Li, Model. Simul. Mater. Sci. Eng. **11**, 173 (2003).
[40] X. Duan, O. Warschkow, A. Soon, B. Delley, and C. Stampfl, Phys. Rev. B **81**, 075430 (2010).
[41] J. Mackenzie, A. Moore, and J. Nicholas, J. Phys. Chem. Sol. **23**, 185 (1962).
[42] Note that Eq. (2) is corrected by a factor of 1/2 from Mackenzie's original paper.[41]